Journal of Structural Dynamics, 2, (pp. 122-143) 2024
Experimentally uncovering isolas via backbone tracking

Journal of Structural Dynamics

Experimentally uncovering isolas via backbone tracking

Lukas Woiwode[1] and Malte Krack *[1]

[1] *University of Stuttgart, Pfaffenwaldring 6, 70569 Stuttgart, Germany*

Abstract

It is known that isolated frequency response branches (isolas) can occur near primary resonances under modal interactions or nonlinear damping. The present work demonstrates how emergence and vanishing of such isolas can be systematically analyzed in an experiment. Feedback control of the phase is employed to track the phase-resonant backbone curve. In addition, the amplitude of the response is controlled, as the excitation level undergoes turning points in the presence of an isola. The acquired data indicates what excitation levels lead to the formation of an isola / its merging with the main branch. Some further analysis of the data permits to characterize possible internal resonances and amplitude-dependent damping. To assess the proposed method, a test rig is considered which involves two similar cantilevered beams undergoing soft collisions via a unilateral spring. A simplified model, which relies on linear modal damping and a massless unilateral spring, suggests that isolas should appear as a result of internal resonances. In contrast, the experiment shows an isola due to nonlinear damping. More specifically, the damping ratio first increases substantially due to the frictional dissipation in inevitable joints. Subsequently, the unilateral interactions scatter energy to other modes (in a non-resonant way), which have much lower damping. This leads to a sudden drop of the effective damping ratio with the amplitude, and leads to the formation of an isola.

Keywords: isolated solutions; detached branches; unilateral contact; non-periodic; nonlinear normal mode;inter-modal targeted energy transfer

Received on November 20, 2023, *Accepted on January 22, 2024*, *Published on January 30, 2024*

1 Introduction

It is an important engineering task to determine how a periodically driven mechanical system responds under variation of the excitation frequency. Sufficiently far away from resonances, the response level is so small that the limit states are close to those of the linearized system. Near resonances, the bifurcation diagram can be much more complicated. Besides turning points and branching points, from which new branches of the same or a different type of limit state emerge, *isolated branches* may exist (Fig. 1-right). These are known by many names, including separated or detached (solution) branches or curves, or islands, or even isolated resonance curves. They are to be distinguished from the *main branch* which continuously extends from the quasi-linear regime. This is also what makes them dangerous: Neither forward/backward stepping of, nor path continuation with respect to the excitation frequency can be expected to be successful in finding the isolated branch.
Typically, isolated branches of periodic frequency responses can be associated with a specific resonance condition. A well-known example are the sub-harmonic resonances of forced-damped single-degree-of-freedom oscillators like the Duffing oscillator, see e. g. the textbook [1]. In the present work, primary resonances are considered, where the excitation frequency is close to a (nonlinear) modal frequency. Two mechanisms can lead to the formation of isolated branches near primary resonances: nonlinear damping and internal resonances. Concerning the former mechanism, including a fundamental example and qualitative analysis the reader is referred to a recent article by Habib et al. [2].

*krack@ila.uni-stuttgart.de

To qualitatively reproduce the latter mechanism, one requires at least another mode. For a fundamental example and some qualitative analysis, the reader is referred to Mangussi and Zanette [3]. Like the primary resonance condition, the internal resonance condition (e. g. $1 : N$ ratio between modal frequencies, where N is an integer) may occur near the equilibrium or at higher energy levels. The internal resonance condition opens the door for a strong dynamic interaction among the modes.

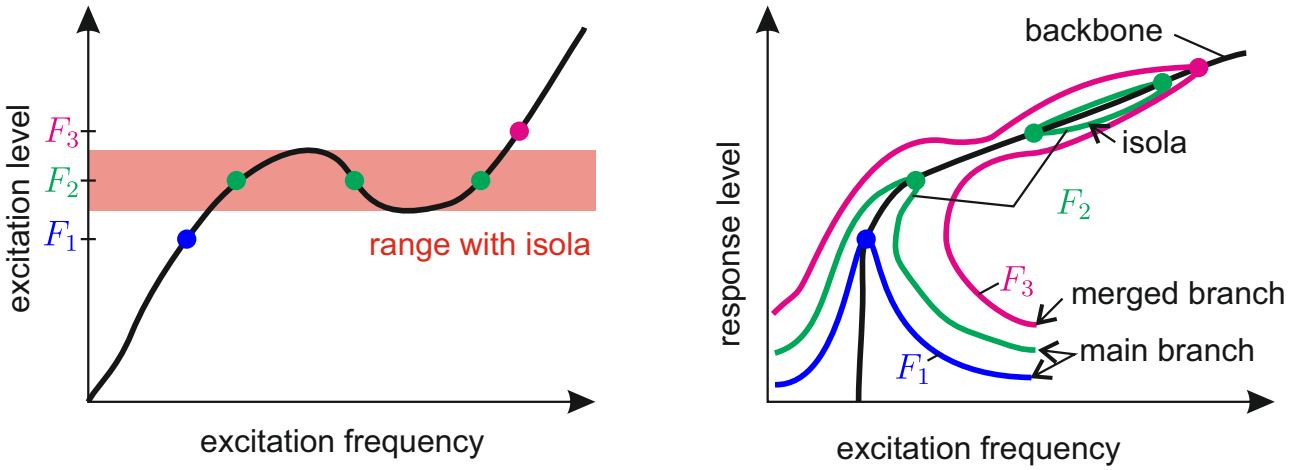

Fig. 1: Idea of proposed method: (left) excitation level vs. frequency relation along backbone; (right) backbone and frequency responses for different excitation levels.

Interestingly, most research focused only on one of the two mechanisms (nonlinear damping OR internal resonances). An important reason for this is probably that damping has the tendency to mitigate (internal) resonance phenomena. Research on isolated branches due to internal resonances has focused on very lightly and typically linearly damped systems. Numerical examples include beams and arches subjected to geometric nonlinearity, or chains of two or more oscillators with a cubic spring. Some analytical investigations based on the method of multiple scales have also been carried out [3, 4]. For lightly-damped systems, the isolated branches appear along the backbones of the unforced-undamped system (nonlinear normal modes). Usually, the isolated branch merges with the main branch at higher excitation levels, as illustrated in Fig. 1. To determine where the frequency response curves of the forced-damped system intersect, an energy-based criterion has been proposed [5, 6]. This criterion requires the balance between power exchanged with the system by forcing and (linear) damping in period average. This is closely linked to the Melnikov function analysis proposed in [7]. There, damping is also assumed as a small perturbation, but allowed to be either linear or nonlinear. It is useful to note that both techniques require the strict separability of strong stiffness and weak damping nonlinearity. This condition is of course not satisfied for any system where hysteretic behavior, e. g. frictional contact is an important source of nonlinearity.

It should be emphasized that different definitions of backbones are commonly used. Above, the backbones of a system in its unforced-undamped configuration were mentioned. One can also define the locus of a certain resonance peak (local amplitude maximum of a frequency response curve) as function of an excitation level as a backbone. Finally, one can define a backbone by the condition of phase resonance. The latter two definitions refer to the forced-damped configuration of the system. All three types of backbones may deviate considerably for finite damping, see e. g. [8]. In the present work, only the phase-resonant backbone plays a role.

Detecting and obtaining a first point on an isolated branch is generally challenging, in particular in the case of high-dimensional systems and limited differentiability (e. g. contact). Here, the reader is referred to a recent overview [9]. Further, it should be remarked that besides isolated branches, Torus bifurcations are often observed in the given scenario (internal resonance), giving rise to windows of quasi-/non-periodic response. One of the first analytical-numerical works in this area is that in [10], and experimental evidence is given in [11]. Finally, it should be stressed that the present work considers isolated branches of frequency response curves only, while isolated branches appear also in the self-excited case, and in the free response case, see e. g. [12, 13].

The experimental analysis of isolated branches is only scarcely addressed in the literature available today. The fact that the isolated branch usually merges with the main branch at higher excitation levels can be exploited to find evidence of isolas in a physical experiment. To this end, the excitation frequency is slowly swept or stepped forward or backward at different excitation levels [14, 15, 16, 17]. The sudden change of the largest response level (and the corresponding excitation frequency) reached in this way, under a small variation of the excitation level is an indication

for the merging of an isolated with the main branch. A very fine variation of the excitation level was used in [16] to clearly resolve the jump in the maximum response level and the associated frequency. To actually reach the isolated branch (for an excitation level where it is detached from the main branch), an impulsive perturbation was proposed in [14]. As an alternative, an appropriate section of the frequency response surface (spanned by excitation frequency and excitation level) can be obtained, and the frequency response curves, including the isolated ones, are derived by interpolation for a given excitation level [17]. To obtain an appropriate section of the frequency response surface, it is important to control the response level. This can be easily inferred from Fig. 1-left: As turning points occur with respect to the excitation level, a simple forward/backward stepping of the excitation level generally does not yield a complete picture. For instance, the excitation frequency can be fixed and the target value of the response level is stepped [17]. To directly obtain a complete isolated branch, control-based path continuation (CBC) can be used. This was applied in [18] to an isolated branch associated with the sub-harmonic resonance of a single-degree-of-freedom oscillator undergoing impacts. An important limitation of that work is that the applied excitation was not controlled, but only the voltage input level to the excitation system was kept fixed. As is well-known in (linear) structural dynamics, due to the change of the system boundaries, the resulting frequency response then inherits properties of the excitation system (e. g. nonlinearity, time-variance). Depending on the load application to the structure under test, the dynamic properties of the exciter (including the mass ratio between the structure and the dynamic mass of the exciter), this can have a crucial influence on both the apparent modal stiffness and the damping. In other words, if the system with fixed input voltage level has an isolated branch, this does not mean that the structure under test with a fixed level of the applied load has an isolated branch. This is the reason why a specifically designed mechanical exciter (Scotch yoke flywheel) was used in [16]. In [14], a fixed applied force level was ensured using feedback control. In fact, not only the fundamental harmonic was controlled but also higher harmonics were compensated using the method proposed in [19]. Higher harmonics can in general distort the dynamics, e. g. change asymptotic stability of limit states, especially under internal resonance conditions [17].
The purpose of the present work is to propose and assess a method for experimental analysis of isolated branches, as outlined in Section 2. This is followed by a numerical illustration in Section 3. The test rig is described in Section 4, followed by the experimental validation of the proposed method in Section 5. Concluding remarks are given in Section 6.

2 Proposed experimental methodology

The proposed method for the experimental analysis of isolated branches relies on tracking the phase-resonant backbone. This is conveniently implemented using a phase-locked-loop controller. As the backbone is obtained in the system's forced and damped configuration, the frequency response curves at a given excitation level are guaranteed to intersect with it. In contrast to previous work, thus, we do not require the separability of stiffness and damping nonlinearity or even linear damping, and we do not intend to track the backbone of the underlying conservative system. By monitoring the excitation level needed to reach a certain point along the backbone, one can simply identify the ranges of the excitation level leading to isolated branches (Fig. 1). By postprocessing the acquired data, one can further identify the contributions of different (linear) modes to different harmonics, in order to characterize potential interactions among internally-resonant modes, and associate them, if applicable, to the formed isolas. On the other hand, if the isolated branch is not due to strong modal interaction, one can obtain a meaningful damping measure as function of the response level, as explained below. The proposed method does not distinguish different sources of nonlinearity or damping. This is viewed both as a strength (broad applicability) and a weakness (limited insight into physical causes).
The control scheme is outlined in Subsection 2.1. The identification of the individual modal and harmonic contributions is explained in Section 2.2. The identification of an effective modal damping ratio is presented in Section 2.3.

2.1 Control scheme

The control scheme for tracking the phase-resonant backbone, including the phase-locked loop, is illustrated in Fig. 2. Herein, SUT stands for structure under test. It is assumed that the excitation is provided either by mounting the structure onto the armature or a slip table attached to a vibration exciter (base excitation), or by applying a concentrated force via a vibration exciter and a stinger (shaker-stinger excitation). The response of the structure is acquired using suitable sensors. For base excitation, as in the case of the test rig considered in the present work, the excitation signal is the base motion. For shaker-stinger excitation, in contrast, the excitation signal is the force applied to the structure under test. In any case, an essentially harmonic voltage signal, amplitude U, phase τ, is input to the

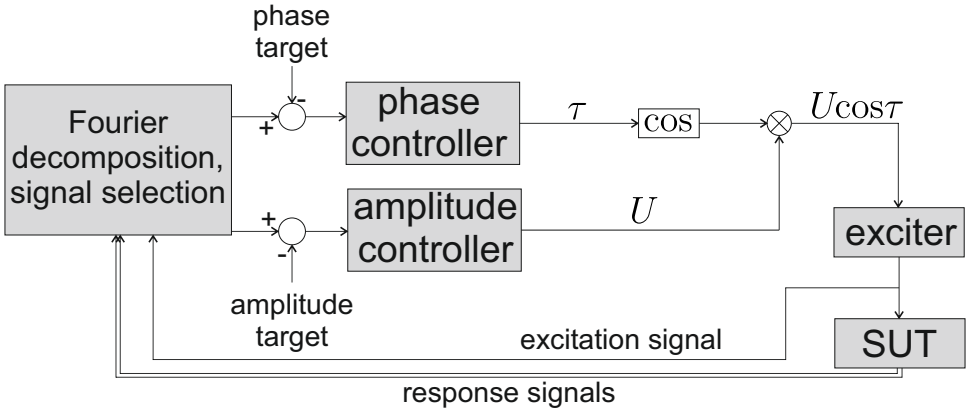

Fig. 2: Proposed control scheme. SUT: structure under test.

(amplifier of the) exciter. The phase controller adjusts the frequency until the specified phase target is reached. The amplitude controller adjusts U until the specified amplitude target is reached.
The key element of the proposed excitation control is a means to estimate the Fourier coefficients of a given signal. This is crucial to determine the phase difference to resonance. It is also used for the amplitude control of the response / excitation. Most previous works used synchronous demodulation for Fourier decomposition. In our experience, using an adaptive filter instead leads to much higher robustness with respect to noise. Phase-locked loop and adaptive filters are quite common in electrical and control engineering. The phase-locked loop has been proposed for nonlinear vibration testing, for the first time, by Mojrzisch et al. [20] and recently gained popularity for backbone tracking [21, 22, 23, 24, 25, 26]. Adaptive filters have been proposed for nonlinear vibration testing, for the first time, by Abeloos et al. [27].
For a signal v, the differential equation of the adaptive filter is

$$\dot{\boldsymbol{V}} = \mu \boldsymbol{h}(t) \left(v - \boldsymbol{h}^{\mathrm{T}}(t)\, \boldsymbol{V} \right), \tag{1}$$

where overdot denotes derivative with respect to time t, $\boldsymbol{h} = [1; \cos\tau; \sin\tau; \ldots; \sin(H\tau)]$, and $\boldsymbol{V} = [V_0; V_{\mathrm{c},1}; V_{\mathrm{s},1}; \ldots; V_{\mathrm{s},H}]$ with the semicolon denoting vertical concatenation. Herein, H denotes the harmonic order and $6/\mu$ corresponds to the $5\ \%$ settling time of the adaptive filter.
The phase lag error is the phase lag between the fundamental harmonic of the excitation signal and the fundamental harmonic of a selected response signal, minus the target phase lag. The phase lag error is used as input to a controller; the output is fed to a voltage controlled oscillator, which corresponds to taking the cosine of the control output. This is multiplied by U, which is the output of the amplitude controller, forming the voltage input to the exciter. Amplitude control is applied for two different purposes in the present work: For the actual backbone tracking, the response amplitude is controlled to a specified value; for some validation tests, the excitation amplitude is kept constant instead. The amplitude controller receives the amplitude of the fundamental harmonic of the excitation signal / response signal, minus the target value, as input.

2.2 Identification of modal and harmonic contributions

Once the transients have decayed sufficiently, the excitation (angular) frequency Ω is time-constant, where $\Omega = \dot{\tau} = \mathrm{const}$. The focus of the present work is on periodic response regimes with the same fundamental frequency Ω. By recording a sufficiently long section of the steady state, the Fourier coefficients of the excitation and the response signals can be obtained. To this end, a discrete Fourier transform is proposed, and integration to displacement level is done in the frequency domain. Denoting $\boldsymbol{q}(t)$ the vector of physical displacements at the sensor locations, one thus obtains the Fourier decomposition,

$$\boldsymbol{q} \quad = \quad \Re\{\sum_{h=1}^{H} \hat{\boldsymbol{q}}(h) \mathrm{e}^{\mathrm{i}h\Omega t}\}, \tag{2}$$

with the harmonic truncation order H and the complex Fourier coefficient vectors $\hat{\boldsymbol{q}}(h)$.
For the following development, it is useful to estimate the modal contributions. To this end, a least-squares fit is

employed. More specifically, the Fourier coefficient vectors of the modal coordinates, $\hat{\boldsymbol{\eta}}(h) = [\hat{\eta}_1(h); \ldots; \hat{\eta}_M(h)]$, with respect to mass-normalized modal deflection shapes are obtained by

$$\hat{\boldsymbol{\eta}}(h) = \overline{\boldsymbol{\Phi}}^{+} \hat{\boldsymbol{q}}(h) \quad h = 1, \ldots, H\,, \tag{3}$$

where $\overline{\boldsymbol{\Phi}}$ is the modal matrix, containing the entries of a suitable set of M mass-normalized modal deflection shapes at the sensor locations as columns, and $\square^{+}$ denotes the Moore-Penrose inverse. The selected set of linear modes should be suitable in the sense that they should span, with sufficient accuracy, the nonlinear vibration response of interest. Selecting all modes of the structure under test that have their frequency in the expected band of the response spectrum, and cannot be excluded due to orthogonality/symmetry reasons, is a practical approach. To obtain a robust and accurate estimation of the individual modal contributions, a sufficiently large number of properly placed sensors is required. The modal frequencies, $\omega_1, \ldots, \omega_M$, and deflection shapes can be obtained from conventional linear modal analysis.
The period-average of the mechanical energy, E_{mech}, within the structure under test can be expressed as

$$E_{\text{mech}} = \sum_{m=1}^{M} \sum_{h=0}^{H} \underbrace{\frac{1}{4}\left[(h\Omega)^2 + \omega_m^2\right] |\hat{\eta}_m(h)|^2}_{E(m,h)}\,. \tag{4}$$

$E(m,h)$ is the contribution of mode m and harmonic h to E_{mech}.
In the linear case, under primary resonance with a lightly damped, well-separated mode, the mechanical energy is expected to be localized in the corresponding mode. Thus, $E(m,1) \neq 0$ for the corresponding mode order m, while all other modal and contributions vanish. When a $1:h$ internal resonance occurs with mode number n along the backbone, $E(n,h)/E(m,1)$ is expected to feature a resonance peak. Hence, monitoring the individual modal and harmonic contributions, permits to detect and characterize potential interactions among internally-resonant modes, and to associate them, if applicable, to the formation of possible isolas.

2.3 Identification of amplitude-dependent modal damping ratio

As mentioned before, there are two possible causes for isolated branches, the resonant interaction among different modes, and nonlinear damping. The method described in Subsection 2.2 permits to analyze if a given isolated branch is formed by a resonant modal interaction. If strong modal interactions remain absent, on the other hand, this means that the vibration energy is confined to a single (nonlinear) mode. In that case, a meaningful damping measure in accordance with the Extended Periodic Motion Concept can be extracted from the phase-resonant backbone as shown in [24, 28]. The modal damping ratio D can be expressed as:

$$D = \frac{1}{2} \frac{\Re\{(\hat{\boldsymbol{\eta}}(1))^{\mathrm{H}} \boldsymbol{\Phi}^{\mathrm{H}} \hat{\boldsymbol{f}}(1)\}}{\Omega^2 \|\hat{\boldsymbol{\eta}}(1)\|^2}\,. \tag{5}$$

Herein, $\square^{\mathrm{H}}$ denotes the Hermitian (complex-conjugate) transpose, and $\hat{\boldsymbol{f}}(1)$ is the complex fundamental Fourier coefficient of the applied forcing. $\boldsymbol{\Phi}$ is the modal matrix in the coordinate system in which the applied forcing is defined, which may generally differ from that of the sensor coordinates, in which $\overline{\boldsymbol{\Phi}}$ is defined. In accordance with the Extended Periodic Motion Concept, the expression in Eq. (5) assumes light damping, but accounts for possible changes of the modal deflection shape, in terms of magnitude and phase of the different linear modal contributions (allowing non-trivial phase lags among the coordinates). Recall that Ω is an output of the phase controller and $\hat{\boldsymbol{\eta}}(1)$ is available from Eq. (3). In the case of shaker-stinger excitation, the applied forcing is usually measured so that $\hat{\boldsymbol{f}}(1)$ can be easily determined. In the case of base excitation, as in the test rig considered later, the applied forcing cannot be directly measured, and Eq. (5) is replaced by a slightly modified expression, as detailed in Subsection 5.1. In either case, one obtains the modal damping ratio for each point along the phase-resonant backbone.
Under the hypothesis that strong modal interactions are absent, the system should behave like a single nonlinear modal oscillator; i. e., Single-Nonlinear-Mode Theory should apply [29]. Besides the analysis of the modal and harmonic contributions in Subsection 2.2, this hypothesis can be checked as follows. The steady-state response of a single nonlinear modal oscillator to an applied forcing with fundamental Fourier coefficient $\hat{\boldsymbol{f}}(1)$ is governed by

$$\left(-\Omega^2 + 2D\omega \mathrm{i}\Omega + \omega^2\right) a \mathrm{e}^{\mathrm{i}\theta} = \boldsymbol{\varphi}^{\mathrm{H}} \hat{\boldsymbol{f}}(1)\,. \tag{6}$$

Herein, D, ω and $\boldsymbol{\varphi}$ are amplitude-dependent modal quantities, and it holds that $\boldsymbol{\Phi}\hat{\boldsymbol{\eta}}(1) = \boldsymbol{\varphi} a$, $\boldsymbol{\varphi}^{\mathrm{H}} \boldsymbol{M} \boldsymbol{\varphi} = 1$, and thus $a^2 = \|\hat{\boldsymbol{\eta}}(1)\|^2$. Those quantities are readily available for each point on the backbone. Eq. (6) can be solved in closed

form for the excitation frequency Ω for a given forcing $\hat{f}\,(1)$ [25]. Thus, isolated frequency response branches can be obtained in a straight-forward way. By synthesizing frequency response curves at different excitation levels, using the above described theory, and comparing to frequency response tests, one can analyze to what extent the observed behavior, in particular the formation of isolas, can be explained by Single-Nonlinear-Mode Theory.

3 Numerical illustration of proposed method

All previous experimental studies on isolated branches along backbones considered cubic-degree polynomial stiffness nonlinearity, and took special care to tune the structure very close to a 1:1 or 1:3 internal resonance. In contrast, a unilateral spring nonlinearity is considered in the present work, and no such tuning was applied. The considered test case comprises two cantilevered beams that may interact via an initially open unilateral spring (Fig. 3). The system is almost symmetric, but the frequencies of the two beams' fundamental bending mode are actually about $10\ \%$ apart. This de-tuning was done deliberately to analyze the hypothesis that the formation of isolas does not require the underlying linear system (at asymptotic vibration levels) to be in internal resonance, provided that the nonlinearity is sufficiently strong (at higher vibration levels). Many examples of almost symmetric systems can be found in engineering, including cables, transmission lines, coupled pendulums, bladed disks, circular/rectangular plates, and rotors. (Soft) collisions, which occur via a unilateral spring in the considered test rig, are typical for opening-closing contacts which appear, for instance, due to free play in clamping or bearing assemblies, or in other mechanical connections. A moderately soft contact (via a spring) instead of a rigid contact is intended in the present work, as it was found that a very stiff spring leads to very narrow parameter windows of periodic vibrations.

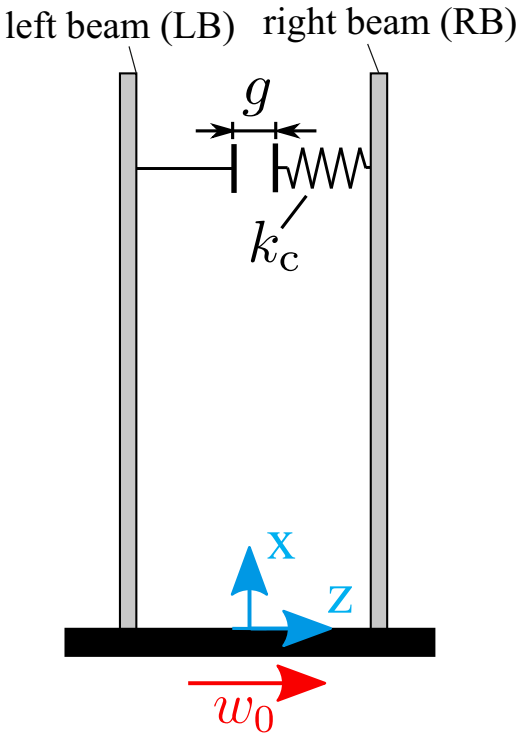

Fig. 3: Schematic illustration of considered problem setting.

The purpose of the present section is to illustrate the proposed method under idealized conditions. It also helps to interpret the results obtained for the actual test rig, and to investigate the dependence on parameters that cannot be easily varied in the physical experiment (e. g. damping). In particular, it will be shown that isolated branches are expected due to internal resonances, for *linear modal damping* and a *massless unilateral spring*.

3.1 Modeling and simulation approach

The elastic displacement, w, in the z-direction of left and right beam is described in terms of Euler-Bernoulli theory. A homogeneous cross section (area A, area moment of inertia I with respect to bending about the y-axis) is considered

along the length L. w is counted relative to the imposed base motion $w_0(t)$; i. e., the total displacement with respect to the inertial frame of reference is $w + w_0$. The continuous beam models are truncated in terms of their mass-normalized clamped-free (linear) normal modes $\varphi_m^{\mathrm{LB}}(x)$ (left beam), $\varphi_m^{\mathrm{RB}}(x)$ (right beam):

$$w^{\mathrm{LB}}(x,t) = \sum_{m=1}^{M} \varphi_m^{\mathrm{LB}}(x)\eta_m^{\mathrm{LB}}(t)\,, \tag{7}$$

$$w^{\mathrm{RB}}(x,t) = \sum_{m=1}^{M} \varphi_m^{\mathrm{RB}}(x)\eta_m^{\mathrm{RB}}(t)\,, \tag{8}$$

$$\ddot{\eta}_m^{\mathrm{LB}} + 2D_m^{\mathrm{LB}}\omega_m^{\mathrm{LB}}\dot{\eta}_m^{\mathrm{LB}} + \left(\omega_m^{\mathrm{LB}}\right)^2 \eta_m^{\mathrm{LB}} + \varphi_m^{\mathrm{LB}}(x_{\mathrm{c}}^{\mathrm{LB}})f_{\mathrm{c}} = \gamma_m^{\mathrm{LB}}\ddot{w}_0(t) \quad m = 1,\ldots,M\,, \tag{9}$$

$$\ddot{\eta}_m^{\mathrm{RB}} + 2D_m^{\mathrm{RB}}\omega_m^{\mathrm{RB}}\dot{\eta}_m^{\mathrm{RB}} + \left(\omega_m^{\mathrm{RB}}\right)^2 \eta_m^{\mathrm{RB}} - \varphi_m^{\mathrm{RB}}(x_{\mathrm{c}}^{\mathrm{RB}})f_{\mathrm{c}} = \gamma_m^{\mathrm{RB}}\ddot{w}_0(t) \quad m = 1,\ldots,M\,, \tag{10}$$

$$f_{\mathrm{c}} = k_{\mathrm{c}} \max\left(q_{\mathrm{c}} - g, 0\right)\,, \tag{11}$$

$$q_{\mathrm{c}} = \sum_{m=1}^{M} \varphi_m^{\mathrm{LB}}(x_{\mathrm{c}}^{\mathrm{LB}})\eta_m^{\mathrm{LB}} - \varphi_m^{\mathrm{RB}}(x_{\mathrm{c}}^{\mathrm{RB}})\eta_m^{\mathrm{RB}}\,. \tag{12}$$

Herein, M is the modal truncation order, and η_m^{LB} and η_m^{RB} are the left and right beam's modal coordinates. The modal forcing term is $\gamma_m^{\mathrm{LB}} = -\rho A \int_0^L \varphi_m^{\mathrm{LB}}\mathrm{d}x$ and analogous for the right beam. $x_{\mathrm{c}}^{\mathrm{LB}}$ and $x_{\mathrm{c}}^{\mathrm{RB}}$ correspond to the location where the unilateral spring is attached to the right and interacts with the left beam. The force in the unilateral spring, f_{c}, defined in Eq. (11), depends on the stiffness k_{c}, the gap g, and the relative displacement q_{c}, which is defined in Eq. (12) in full accordance with the modal truncation. Based on a modal convergence study, the four lowest-frequency bending modes of each beam are retained; i. e., $M = 4$. Linear modal damping is assumed.
Harmonic base motion is assumed, with the acceleration $\ddot{w}_0 = a_{\mathrm{exc}}\cos(\Omega t)$. The harmonic balance method is used to compute periodic responses with the fundamental period of the excitation. Accordingly, the response is approximated in the form of a Fourier series,

$$\eta_m = \Re\{\sum_{h=1}^{H} \hat{\eta}_m(h)\mathrm{e}^{\mathrm{i}h\Omega t}\}\,, \tag{13}$$

truncated to order H, for $m = 1,\ldots,M$, left and right beam. Substituting this into Eqs. (9)-(10), one obtains a residual. Harmonic balance requires that the Fourier coefficients of this residual vanish up to the same order H. This yields an algebraic equation system for the unknown Fourier coefficients $\hat{\eta}_m(0)$ to $\hat{\eta}_m(H)$, $m = 1,\ldots,M$, left and right beam. The linear part of Eqs. (9)-(10) can be cast quite easily into the frequency domain. To evaluate the Fourier coefficients of the nonlinear term f_{c}, the alternating frequency-time scheme is used. The implementation is based on the tool NLvib [30]. Phase resonance with respect to the fundamental harmonic between q_{c} and the base motion is imposed as an additional equation, and the excitation frequency Ω is treated as an additional unknown. The amplitude of the harmonic base acceleration, a_{exc}, is also considered as a free parameter, and the backbone curve is computed using numerical path continuation. Here, a tangent predictor is combined with a pseudo-arc length parametrization. A Newton-type method is used to solve the resulting nonlinear algebraic equation system. Based on a harmonic convergence study, a truncation order of $H = 40$ was selected.

3.2 Numerical results: mode 1

The nominal parameter values throughout this section are consistent with the actual test rig presented in Section 4. In particular, the modal frequencies ω_m^{LB}, ω_m^{RB} and damping ratios D_m^{LB}, D_m^{RB} are set to those obtained from linear modal testing (Tab. 1), and the parameters ρA, L, $x_{\mathrm{c}}^{\mathrm{LB}}$, $x_{\mathrm{c}}^{\mathrm{RB}}$, k_{c} and g are set according to the test rig design. Those parameters were varied in a wide range and it was found that the selected nominal values indeed lead to representative numerical results. In fact, further numerical studies (results not shown for brevity) indicate that the existence of isolated branches is quite insensitive to the excitation scenario (base excitation vs. concentrated force applied to one of the beams).
The backbone curve departing from ω_1^{RB} is depicted in Fig. 4. For sufficiently small vibrations, the unilateral spring is inactive, resulting in linear behavior with a constant frequency $\Omega = \omega_1^{\mathrm{RB}}$. As soon as $q_{\mathrm{c,max}} = g$, the unilateral spring is activated, leading to an increased effective stiffness (hardening effect), and thus the backbone turns towards the right. Here, $q_{\mathrm{c,max}}$ is the maximum of q_{c} reached over a sufficiently long section of the steady state. For large vibrations, a vertical asymptote seems to be approached.

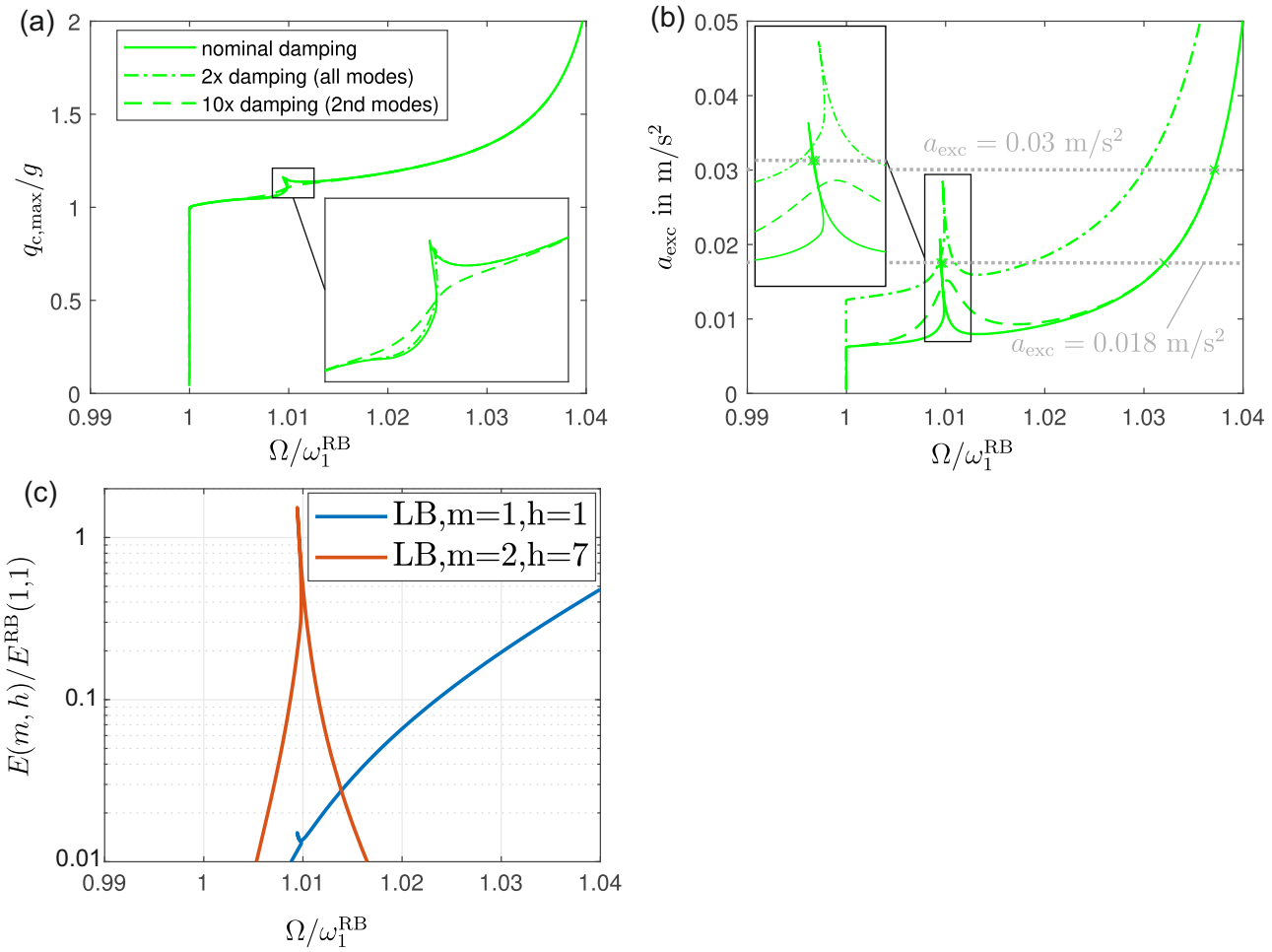

Fig. 4: Simulated backbone departing from ω_1^{RB}: (a) response level vs. excitation frequency; (b) excitation level vs. excitation frequency; (c) dominant modal and harmonic contributions to vibration energy for nominal damping as specified in Tab. 1.

Near $\Omega/\omega_1^{\mathrm{RB}} = 1.01$, a special feature appears in Fig. 4a. In that region, the excitation level exhibits a local peak, yielding two turning points in Fig. 4b. In this example, a $1:7$ interaction between the directly-driven first bending mode ($m = 1$) of the right beam, and the second bending mode ($m = 2$) of the left beam was found to be responsible for this behavior. This can be best inferred from Fig. 4c, where the individual contributions to the mechanical energy according to Eq. (4) are depicted. Recall that $E(m,h)$ is the contribution of mode m and harmonic h to E_{mech}. These contributions were calculated for both beams, and normalized by the contribution of the directly-driven mode and harmonic, $E^{\mathrm{RB}}(1,1)$. The only contributions that exceed 1 % of $E^{\mathrm{RB}}(1,1)$ are those depicted in Fig. 4c, $E^{\mathrm{LB}}(1,1)$ and $E^{\mathrm{LB}}(2,7)$. Of these, only $E^{\mathrm{LB}}(2,7)$ shows a pronounced resonance peak, which confirms the above stated modal interaction. $E^{\mathrm{LB}}(1,1)$, on the other hand, grows monotonically almost everywhere, which can be interpreted as a continuous change of the modal deflection shape.

Fig. 4a and b also show results for increased damping, in the case where all modes receive twice their nominal damping ratio, and in the case where the second bending modes of left and right beam receive ten times their nominal damping ratio. Interestingly, when all modes receive higher damping, the excitation level vs. frequency curve (Fig. 4b) is shifted/stretched upwards, while the form of the local peak, both in Fig. 4a and b is almost unaffected. In contrast, when only the second bending modes receive higher daming, the backbone in Fig. 4a is almost smooth and the local peak in Fig. 4b is considerably mitigated. For a higher stiffness of the unilateral spring, the hardening and the effects of the resonant modal interaction would be more pronounced, and possibly more internal resonance phenomena would occur.

Frequency responses are depicted in Fig. 5. For $a_{\mathrm{exc}} = 0.018$ m/s^2, an isolated branch appears, while this is merged with the main branch for $a_{\mathrm{exc}} = 0.03$ m/s^2. This is in full accordance with Fig. 4b, where a single intersection with the backbone is obtained for $a_{\mathrm{exc}} = 0.03$ m/s^2, while three intersections are obtained for $a_{\mathrm{exc}} = 0.018$ m/s^2 (cf. also

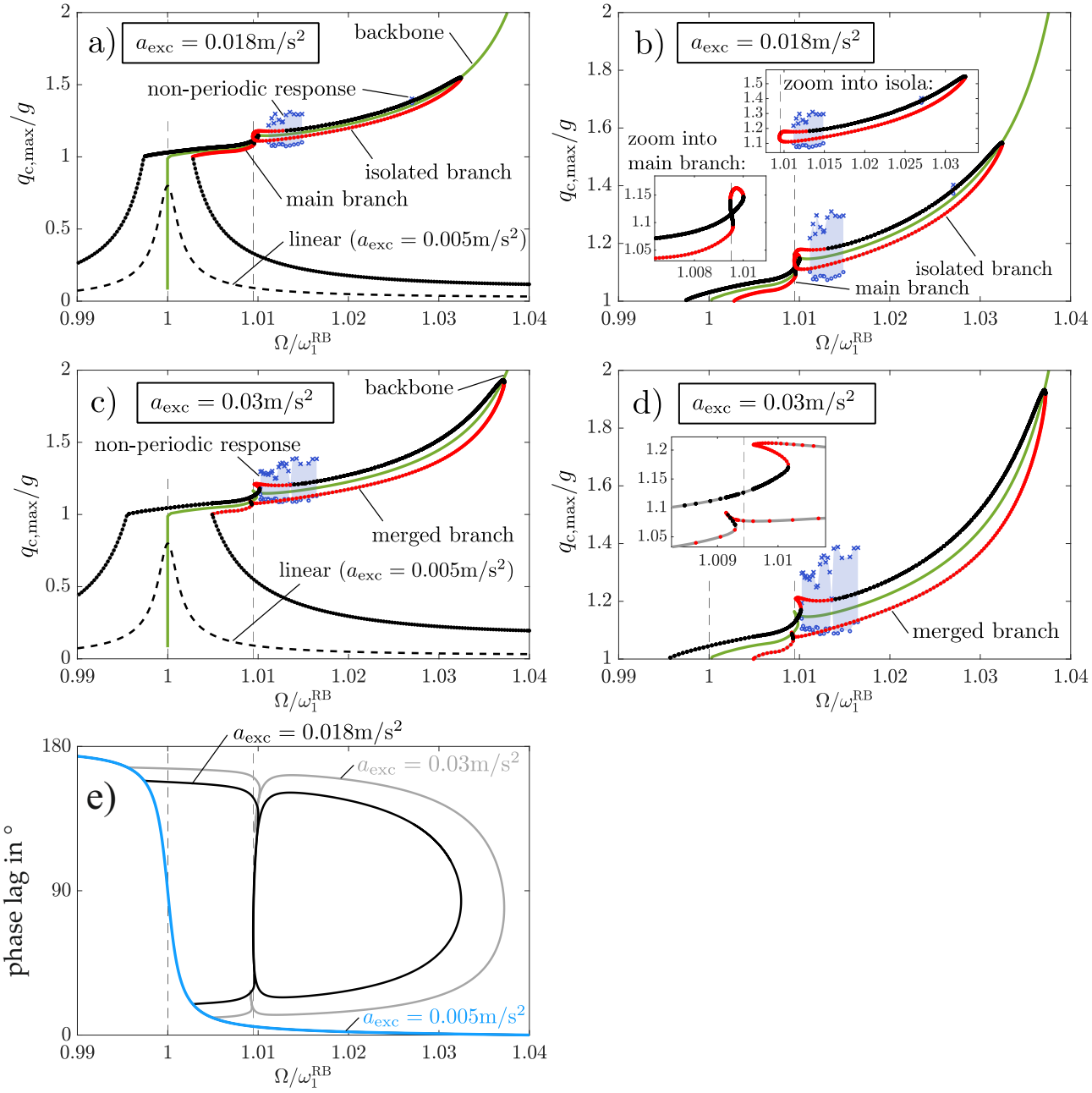

Fig. 5: Simulated frequency response near ω_1^{RB}: (a) and (b) excitation level leading to an isolated branch; (c) and (d) excitation level leading to a merged branch; (e) phase response for different excitation levels. Red markers indicate unstable points (in the sense described in the text). Blue shaded areas indicate the amplitude range of non-periodic limit states. Nominal damping is considered as specified in Tab. 1.

Fig. 1). The isolated branch was simply computed by starting from the backbone, removing the phase constraint and applying path continuation for fixed excitation level. As can be seen in Fig. 5e, the phase response is generally not single-valued anymore, which shows clearly the importance of employing phase control in the experiment.
A practical stability analysis was carried out, where numerical time step integration is initiated from each limit state computed with harmonic balance, for a sufficiently large set of small, random perturbations. If the trajectory did not return sufficiently close to the initial limit state, the corresponding solution point is considered as unstable and marked as red. In the neighborhood of the internal resonance, a window of non-periodic limit states appears. As stated in the introduction, Torus bifurcations are well-known to appear near internal resonances, see e. g. [10, 11]. By determining the largest value of q_{c} in each excitation period, and taking the maximum and the minimum, over a sufficiently large

number of periods of the steady state, the amplitude range of the non-periodic response is obtained (depicted as blue shaded region).

3.3 Numerical results: mode 2

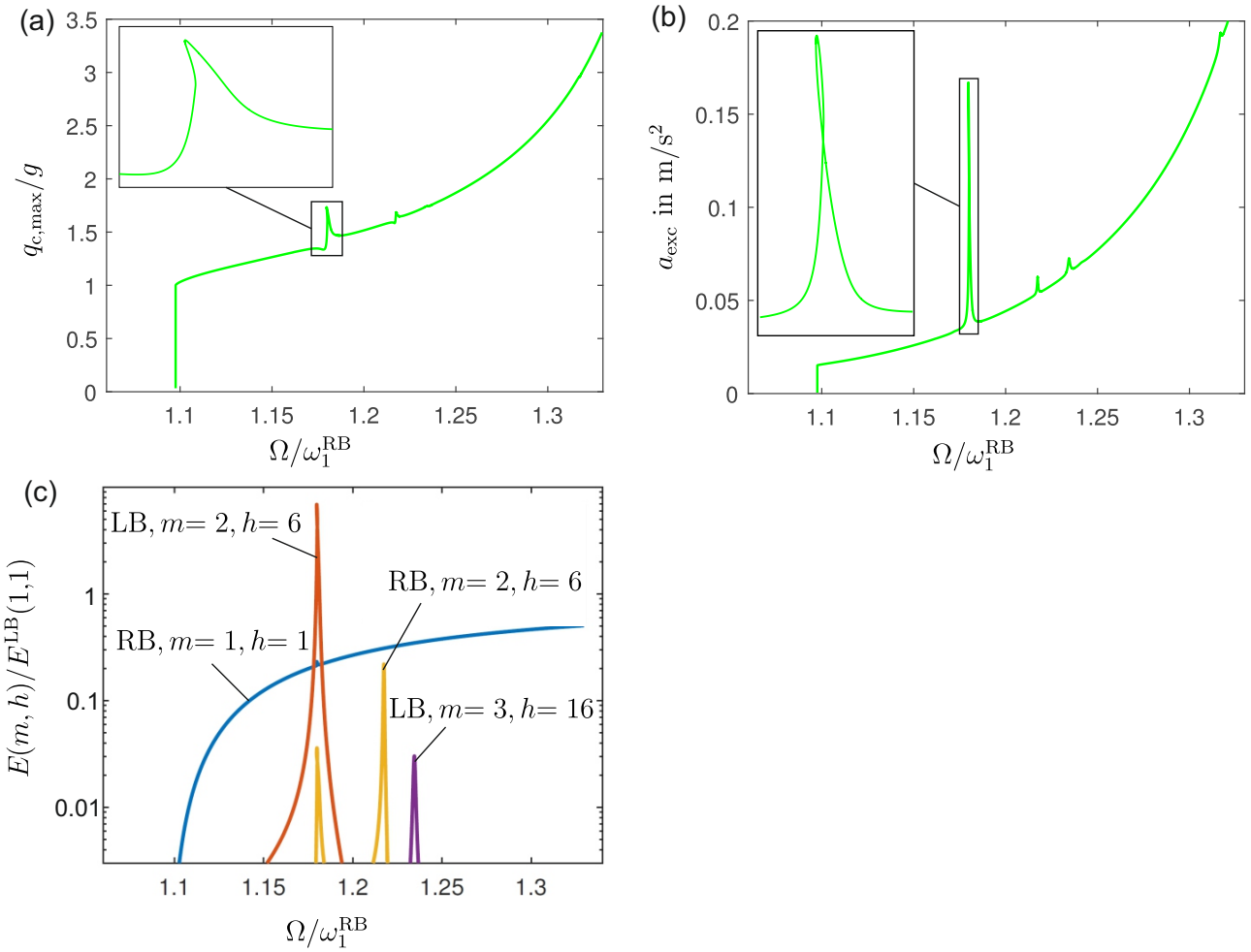

Fig. 6: Simulated backbone departing from ω_1^{LB}: (a) response level vs. excitation frequency; (b) excitation level vs. excitation frequency; (c) dominant modal and harmonic contributions to vibration energy.

The analysis was also carried out for the second mode, i. e., the first bending mode of the left beam. The results are depicted in Fig. 6 and Fig. 7. As this has an about 10 % higher natural frequency, the backbone departs from $\Omega/\omega_1^{RB} \approx 1.1$. The results are largely similar; two important differences should be mentioned: more resonant modal interactions, and more pronounced non-periodic behavior. This is described further in the following two paragraphs. Fig. 6c depicts all contributions that exceed 1 % of $E^{LB}(1,1)$. Three resonant modal interactions appear now in the depicted range, namely a $1:6$ interaction with the second mode of the left beam, and later also with the right beam, and a $1:16$ interaction with the third mode of the left beam. Here, one can observe that the higher the order of the internal resonance, the weaker is its effect. In particular, the range of excitation levels leading to isolated branches becomes smaller and may even be empty (for higher damping). As the effect of the first internal resonance is so strong, there are ranges of the excitation level leading to five intersections in Fig. 6b. Consequently, two isolated branches appear, e. g., for $a_{exc} = 0.06$ m/s^2, as can be seen in Fig. 7a-b.
Non-periodic behavior not only occurs near the mentioned internal resonances in the depicted case. In fact, the response becomes non-periodic as soon as the nonlinear regime is entered. Deep modulations (with almost zero minimal amplitude) are observed over a wide frequency window. A further analysis shows that the first bending modes of both the left and the right beam contribute substantially to this regime. A similar observation was made in

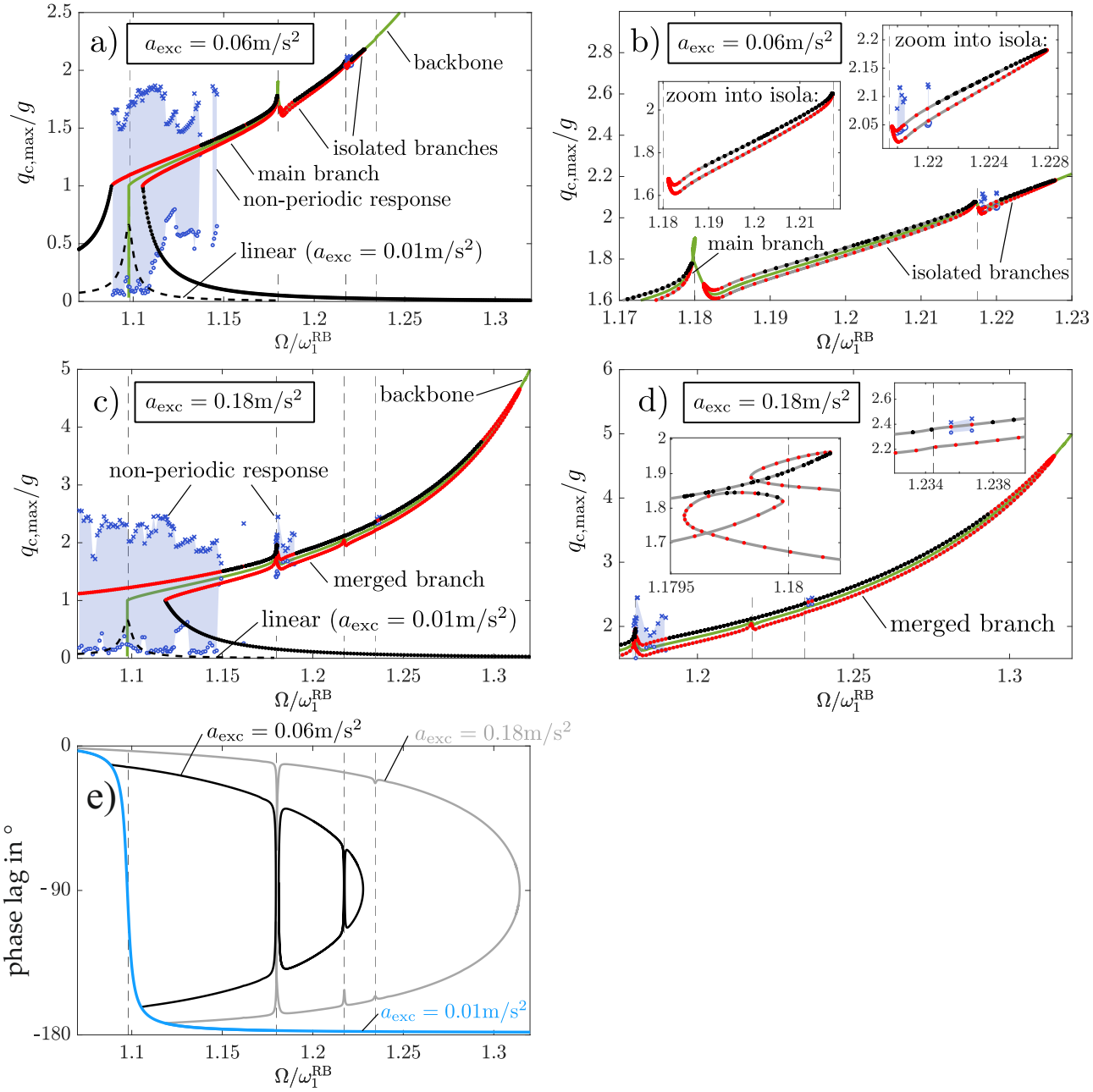

Fig. 7: Simulated frequency response near ω_1^{LB}: (a) and (b) excitation level leading to an isolated branch; (c) and (d) excitation level leading to a merged branch; (e) phase response for different excitation levels.

[31], where a slightly de-tuned, yet essentially symmetric arrangement of two beams undergoing recurrent frictional collisions was considered, and base excitation was applied with a frequency near the second mode.

4 Test rig

The developed test rig implements the schematic shown in Fig. 3. Its design is described next. Subsequently, the results of a linear modal analysis are presented. Finally, the implementation of the control loop is explained.

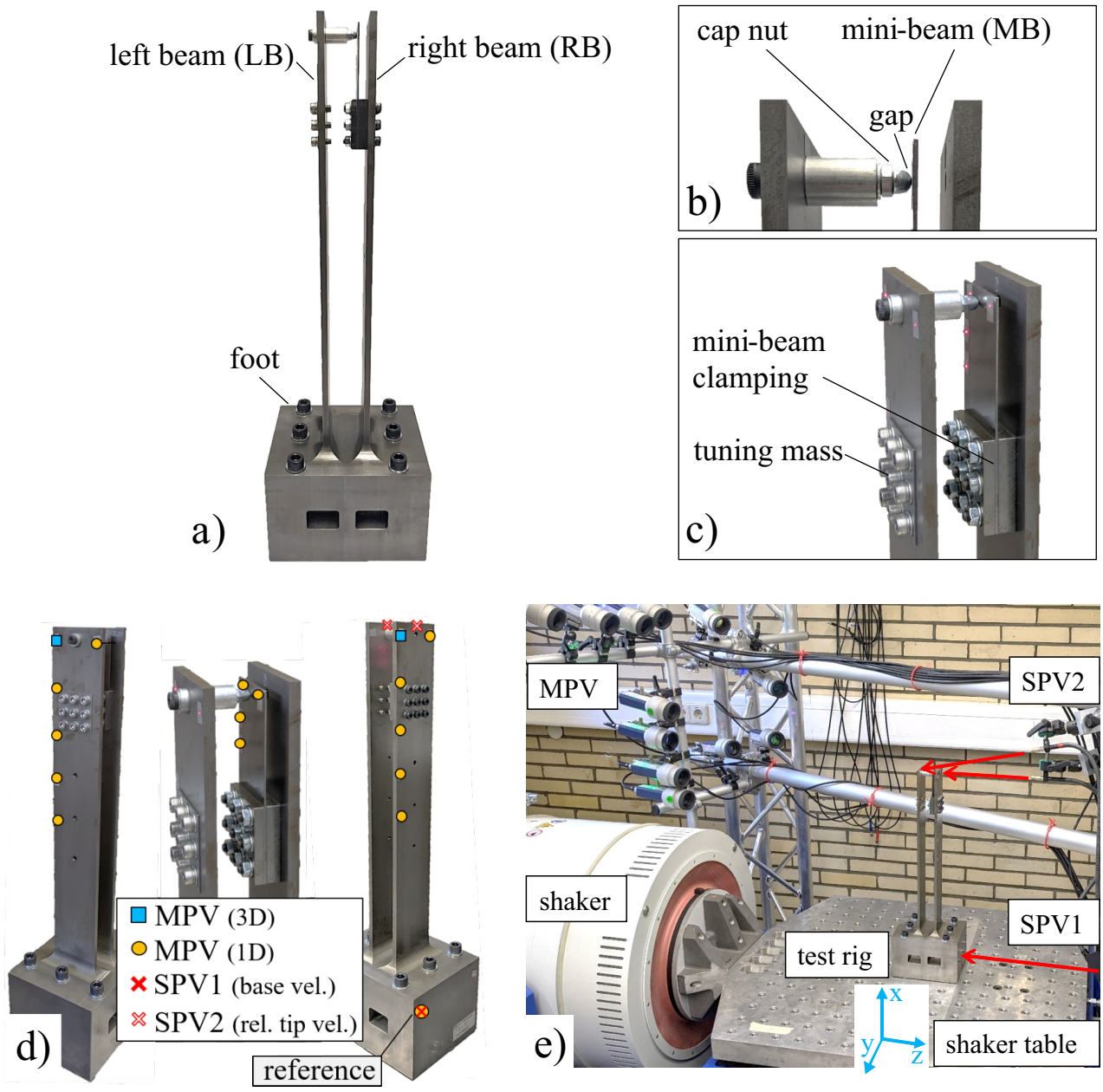

Fig. 8: Test rig: (a) overview of assembled test rig; (b) contact detail; (c) clamping of mini-beam and tuning mass; (d) sensor locations; (e) test rig mounted on shaker table. MPV: Multi-Point Vibrometer; SPV: Single-Point Vibrometer.

4.1 Description of test rig and explanation of its design

As can be seen in Fig. 8a, left and right beam, and the base are manufactured as one monolithic piece using wire erosion. The actual dimensions of the test rig are given in a separate Fig. A.1 so that Figs. 8 is not overcrowded. The intent was to avoid frictional connections as far as possible, as these are an important source of variability and damping nonlinearity. A few connections were deemed inevitable: base to exciter (to apply dynamic loading), unilateral spring to right beam (to adjust the stiffness), contact element to left beam (to adjust the clearance). In addition, the contact partners should be exchangeable in the event of plastic damage / wear. Finally, a tuning mass was mounted on the left beam. This tuning mass was actually used to de-tune the fundamental bending modes away from the 1:1 internal resonance. Thus, the tuning mass could have been avoided (e. g. by changing the cross section of one beam) for the present work, while it is crucial for planned research where the effect of tuning is to be analyzed.
To reduce undesired effects of the connection between structure under test and slip table on the dynamics of interest,

the foot is designed as relatively massive (less strain energy in the frictional contact region). With the same intent, the unilateral spring is mounted between two plates with a relatively high bolt density (9 M5 screws at $6\ \mathrm{Nm}$ nominal torque over the area of $40\ \mathrm{mm} \times 40\ \mathrm{mm}$). The tuning mass consists of a $1\ \mathrm{mm}$ thick square plate, edge length $40\ \mathrm{mm}$, which is also mounted via 9 M5 screws (fine-threaded, $6\ \mathrm{Nm}$ nominal torque), to threaded holes in the left beam.
The unilateral spring is implemented as an additional, $1\ \mathrm{mm}$ thick beam, clamped to the right beam. That beam is referred to as *mini-beam* in the following. For the given dimensions and the material's elastic properties, the effective unilateral spring stiffness is about $15.8\ \mathrm{N/mm}$. Both the main part (left and right beam with base) and the mini-beam are made of steel alloy 42CrMo4+QT. A mounting aid is used to align all components of the mini-beam assembly at the intended height of the right beam.
The left beam can come into contact with the mini-beam via a cap nut (galvanized steel; radius of hemisphere about $2.5\ \mathrm{mm}$) that is mounted onto an M4 fitting screw. An aluminum bushing element is used to ensure a clearance of about $0.15\ \mathrm{mm}$ between cap nut and mini-beam.
The dynamic load is applied in the form of base excitation, by mounting the test rig via 6 M10 screws ($40\ \mathrm{Nm}$ nominal torque) onto the slip table of a large shaker (TIRA S 51010/LS-340, $11\ \mathrm{kN}$ nominal sine force, power amplifier A 1 02 11 021 SV). The ratio between the free part of the test rig (everything without the base), and the total moving mass (base, slip table, shaker armature) is $2.6\ \mathrm{kg}\ /\ 104\ \mathrm{kg}\ = 2.5\ \%$. The low mass ratio reduces undesired feedback of the (nonlinear) vibration on the exciter, and facilitates the control tasks described later.
The vibration was measured using laser Doppler vibrometry. More specifically, the base velocity was measured at the reference point indicated in Fig. 8d using a single-point vibrometer (SPV1, Polytec VibroFlex QTec VFX-I-160; sensitivity $3\ \mathrm{mm/s/V}$). The relative tip velocity was measured using a differential vibrometer (SPV2, Polytec OFV-5000 with a OFV-552-2 laser head, sensitivity $200\ \mathrm{mm/s/V}$). Additionally, a multi-point vibrometer (Polytec MPV-800) was used to measure the velocity at different heights of left, right and mini-beam, as indicated in Fig. 8d. To this end, 22 fiber optic sensor heads were mounted on a rack system that allowed the alignment from various positions around the test rig at a distance of $0.7\ \mathrm{m}$ - $1.0\ \mathrm{m}$. At each measurement point, reflective tape was used to increase the signal-to-noise ratio. In total, velocity data was acquired at 17 measurement points (2 points in 3D, 15 points in 1D). To obtain three-dimensional data, triples of sensor heads were aligned onto the same measurement point. To get the orientation of each sensor head, in the coordinate system shown in Fig. 8e, a geometry sensor (Leica 3D Disto) was used. 3D data was acquired to check whether any imperfections of the excitation system or the test rig led to an unexpected motion component. Indeed, it was verified that the motion in the x- and y-direction is negligible. Thus, for the 1D data, the incline angle was corrected assuming pure motion in the z-direction.
The basic dimensions of the test rig were set to have a natural frequency in the range of $30\ \mathrm{Hz}$. For much lower frequencies, one approaches the operating limit of the excitation system, which starts at $2\ \mathrm{Hz}$, and one may expect lower signal quality of the velocity sensors. For much higher frequencies, the generated higher harmonics could not have been captured accurately with the given real-time system with operates at a sampling frequency of about $8\ \mathrm{kHz}$.

4.2 Linear modal analysis

A linear modal analysis was carried out. Apart from the fact that this is generally good practice before a nonlinear analysis, the identified modal properties were used in the numerical study presented in Section 3. A pseudo-random excitation at $0.1\ \mathrm{V}$ input level to the exciter was applied with a frequency range from $2\ \mathrm{Hz}$ to $1.25\ \mathrm{kHz}$, and a frequency resolution of $24.4\ \mathrm{mHz}$. It was ascertained that the resulting response is sufficiently low not to activate the unilateral spring. The frequency responses of left, right and mini-beam are depicted in Fig. 9. More specifically, the transfer behavior from the base velocity (input) to the elastic tip deflection (relative to the base) on each beam (output) is shown (all in z-direction).

Table 1: Identified linear modal properties.

mode	left beam		mini-beam		right beam	
	$\omega/2\pi$ in Hz	D in %	$\omega/2\pi$ in Hz	D in %	$\omega/2\pi$ in Hz	D in %
1B	30.95	0.20	277.74	0.06	28.20	0.10
2B	199.04	0.02	-	-	205.54	0.03
1T	397.64	0.02	870.00	0.05	379.33	0.07
3B	556.82	0.06	-	-	594.98	0.14
4B	1085.93	0.09	-	-	1168.62	0.23

The frequency response functions exhibit well-separated resonances. Thus, simple single-degree-of-freedom fits

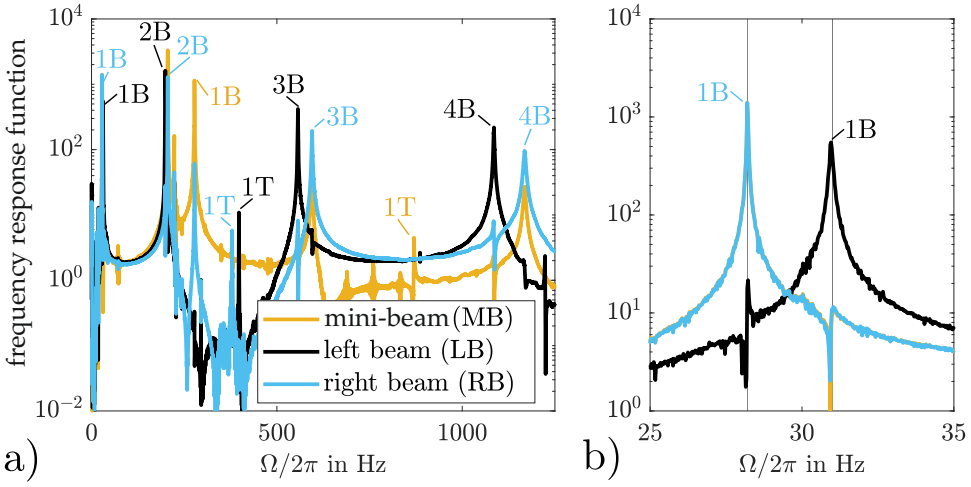

Fig. 9: Frequency response functions of left, right and mini-beam obtained for low excitation level: (a) overview; (b) zoom. 1B through 4B refer to first through fourth bending, 1T refers to first torsion mode.

were found sufficient to identify the modal frequencies and damping ratios listed in Tab. 1. The given frequency range contains the four lowest-frequency bending modes (in the z-direction) and the first torsion mode (around the x-axis), of the left and the right beam. It also contains the lowest-frequency bending and the lowest-frequency torsion modes of the mini-beam. The nonlinear analysis focuses on the lowest-frequency bending mode (1B) of the right beam, at about 30 Hz. With this, it can be inferred that all modal frequencies up to the 40-th multiple of the considered modal frequency are accounted for in the linear modal analysis. Further, one can verify from Tab. 1 that the 1B modal frequency of the left beam is indeed about 10 % higher than that of the right beam. Remarkably, the 1B modal damping ratio of the left beam is about two times higher than that of the right beam, whereas the right beam has higher damping for the remaining modes in the given frequency range. With a few exceptions (3B and 4B of right beam), the higher modes have lower damping ratio than the fundamental ones. Dissipation can generally be due to inelastic processes within the material, the interaction with the ambient air, and frictional contact interactions in the mechanical joints. For steel assemblies, dissipation within the material and due to the ambient air is usually negligible [32], so that the frictional connections are viewed as the main source of dissipation in the present system.

4.3 Implementation of control loop

All control tasks are implemented on a dSPACE MicroLabBox operating at a sampling frequency of about 8 kHz. For the tests in the present work, an adaptive filter with a harmonic order of $H = 10$ is used with a 5 % settling time of $6/\mu = 0.6$ s, which corresponds to about 18 excitation periods. For phase control, a PID controller is used with gains set as $P_{\Delta\Theta} = 14\text{rad/s}$, $I_{\Delta\Theta} = 14\text{rad/s}^2$ and $D_{\Delta\Theta} = -0.1\text{rad}$. For amplitude control, a PI controller is used with the gains $P_a = 20\ \text{V/(m/s}^2)$ and $I_a = 20\ \text{V/(m/s)}$. The same gains are used, both in the case of the excitation amplitude, and in the case of the response amplitude mode of the controller.

The gains of both the phase and the amplitude controller were set heuristically. The intent was to decouple the time scales of the individual controllers. In particular, it was ensured that the amplitude controller is slower than the phase controller. Also, it was ensured that the phase controller is slower than the adaptive filter. Overall this led to a good performance of the nonlinear vibration tests: The maximum phase error was 2.5 % (using $\pi/2$ as reference), and the maximum response amplitude error was 5.5 %. For the frequency response tests, the excitation amplitude was controlled, where the maximum amplitude error was in a similar range when the response was (almost) periodic. In the non-periodic regime, strong and relatively fast response modulations occur. Here, the excitation amplitude control was too slow to compensate the resulting modulation of the excitation amplitude. In the absence of such strongly modulated responses, the above stated errors are below the thresholds proposed in previous works, e. g. the 5 % tolerance deemed acceptable for the phase control in [13]. The control design can thus be regarded as quite successful, especially when considering the challenges generally associated with the control of multi-degree-of-freedom/multi-mode systems subjected to (soft) impacts.

In general, one might be concerned about higher harmonics in the applied excitation. As will be shown, however, strong modal interactions remained absent, so that the structure under test is apparently rather insensitive to higher

harmonics. Consequently, no compensation of higher harmonics was implemented.

5 Experimental analysis of (real) test rig

Based on the results of the numerical analysis, one can expect isolated frequency response branches near the primary resonance of both the first and the second mode. Among the two modes, the first mode shows less complicated dynamics. More specifically, fewer internal resonances occur, and non-periodic behavior appears in more narrow frequency bands. As the focus of the present work is on isolated branches rather than non-periodic behavior, results are shown only for the first mode in this section.

5.1 Experimental results: backbone (mode 1)

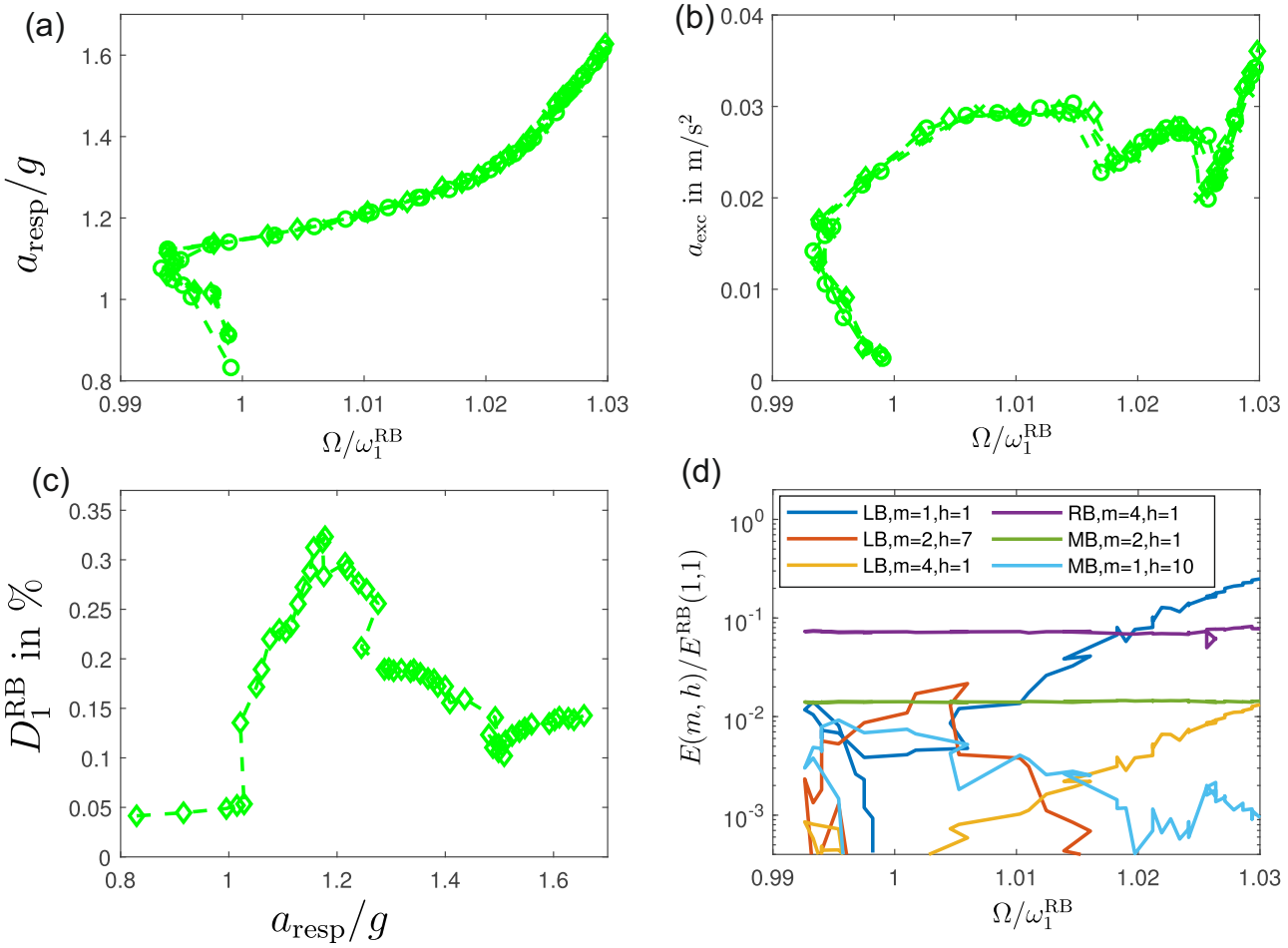

Fig. 10: Measured backbone departing from ω_1^{RB}: (a) response level vs. excitation frequency; (b) excitation level vs. excitation frequency; (c) modal damping ratio vs. response level; (d) dominant modal and harmonic contributions to vibration energy.

The experimental results from the backbone tracking are depicted in Fig. 10. As response measure, the magnitude of the fundamental harmonic of the relative tip displacement, a_{resp}, is used, obtained using the velocity data acquired with SPV2 (Fig. 8d). In Fig. 10a-b, data is plotted for three upward and one downward response amplitude stepping. Apparently, the test is very well repeatable, in spite of potential sources of variability (thermal effects; wear in the frictional connections; impact-induced plasticity). Before the expected hardening at higher amplitudes, a mild softening of about 0.6 % is observed. This is attributed to the frictional contact interactions at the connection between mini-beam and right beam, and between left beam and (de-)tuning mass. More specifically, recurrent opening-closing and stick-slip transitions in parts of the contact area are a plausible explanation for the softening trend. This is in line with [33, 13], where softening-hardening was also observed in the experiment instead of pure hardening theoretically

expected for ideal connections/boundary conditions.
As can be seen in Fig. 10b, turning points occur with respect to the excitation level along the backbone. Thus, in the range $a_{\mathrm{exc}} \in [0.021, 0.030]\ \mathrm{m/s^2}$, isolated frequency response branches are expected. Compared to the numerical results in Fig. 4b, a qualitative difference can be found: The excitation level shows a clear peak towards higher excitation levels in the model, whereas the excitation amplitude first drops and then increases again in reality. This is a first indication that the isolated branches are caused by a different physical phenomenon.
To further investigate the physical cause for the isolated branches, the modal and harmonic contributions to the mechanical energy are analyzed using Eq. (4) and Eq. (3). To set up the matrix $\overline{\boldsymbol{\Phi}}$ in Eq. (3), the mass-normalized modal deflection shapes are required. Mass-normalization is impossible to achieve experimentally in the given case of base excitation, because the excitation force cannot be directly measured. Instead, $\overline{\boldsymbol{\Phi}}$ was obtained from a refined version of the model presented in Section 3. More specifically, the mini-beam was also modeled using Euler-Bernoulli theory. Left, right and mini-beam were all discretized using standard beam elements. Point masses were included to account for the (de-)tuning mass, the cap nut and bushing assembly on the left beam, and the clamping of the mini-beam on the right beam. The point masses were calibrated to achieve very good agreement with the modal frequencies listed in Tab. 1, and it was also ascertained that the resulting mass-normalized modal deflection shapes are well-correlated with the non-normalized ones obtained from the experimental linear modal analysis.
The contributions of individual modes and harmonics to the mechanical energy are depicted in Fig. 10d (for one of the four test runs). All contributions that exceed $0.7\ \%$ of $E^{\mathrm{RB}}(1,1)$ are depicted. With some imagination, one can infer a well-mitigated $1:7$ interaction with the second bending mode ($m=2$) of the left beam near $\Omega/\omega_1^{\mathrm{RB}} = 1.005$. However, there is no visible feature near this point in Fig. 10b. The considerable drops and rises in Fig. 10b occur near $\Omega/\omega_1^{\mathrm{RB}} = 1.017$ and $\Omega/\omega_1^{\mathrm{RB}} = 1.025$. At these frequencies, on the other hand, there is no visible feature in Fig. 10d. Thus, one can exclude that resonant modal interactions are responsible for isolated branches in the experiment.
Ruling out internal resonance phenomena, one can suspect that nonlinear damping causes isolated branches in the test rig. In the case of base excitation, the modal damping ratio from Eq. (5) can be replaced by [28]:

$$D_1^{\mathrm{RB}} = \frac{1}{2} \frac{\left| \left(\hat{\boldsymbol{\eta}}\,(1)\right)^{\mathrm{H}} \boldsymbol{\Phi}^{\mathrm{H}} \boldsymbol{M} \boldsymbol{b} a_{\mathrm{exc}} \right|}{\Omega^2 \| \hat{\boldsymbol{\eta}}\,(1) \|^2} \,. \tag{14}$$

Herein, $\boldsymbol{M}$ is the mass matrix, and $\boldsymbol{b}$ is a Boolean vector with entry one if the corresponding coordinate points in the direction of the base motion, and zero if it points in the orthogonal direction. a_{exc} and Ω are readily available for each point along the backbone, and $\hat{\boldsymbol{\eta}}(1)$ was already obtained via Eq. (3). The term $\boldsymbol{\Phi}^{\mathrm{H}}\boldsymbol{M}\boldsymbol{b}$ is computed with the same model that was used before to obtain $\overline{\boldsymbol{\Phi}}$. $\boldsymbol{\Phi}$ is the modal matrix in the coordinates of the complete (FE) model, while $\overline{\boldsymbol{\Phi}}$ is the restriction to the sensor coordinates. The results are depicted in Fig. 10c.
The modal damping ratio is almost constant for sufficently low amplitudes, where also the frequency is almost constant, suggesting linear behavior. The asymptotic value is about $0.05\ \%$, which is by a factor of about two lower than that identified by linear modal testing listed in Tab. 1. One should remark that a variability of the modal damping ratio in this range is not surprising for a structure with friction joints. In any case, the modal damping ratio increases substantially, here by about a factor of seven. This is typical for dissipation in frictional connections, and is in full accordance with the interpretation of the softening trend. When the unilateral spring nonlinearity becomes important, and leads to considerable hardening, the damping level overall decreases. This is explained by the fact that more energy goes into lighter damped modes. More specifically, at the highest vibration level, $E^{\mathrm{RB}}(1,1)$ only contributes to about $73\ \%$ to the total mechanical energy (instead of $100\ \%$ in the quasi-linear regime). It is important to stress that this energy transfer is not a resonant phenomenon, but rather energy is scattered to many modes due to the (soft) impacts. A large part of those modes has lower damping, at least much lower than the maximum damping ratio of more than $0.3\ \%$ reached near $a_{\mathrm{resp}}/g = 1.2$ (Tab. 1). Apparently, this is the reason for the decrease of the modal damping ratio, and is responsible for the formation of the isola.

5.2 Experimental results: frequency responses (mode 1)

To actually make the isolated frequency response branches visible, two types of additional tests were carried out. First, stepped frequency testing, and, second, stepped phase testing. In both cases, the excitation level was controlled as described in Subsection 2.1. Fig. 11 shows results for two different excitation levels, $a_{\mathrm{exc}} = 0.028\ \mathrm{m/s^2}$, for which an isolated branch appears, and $a_{\mathrm{exc}} = 0.0305\ \mathrm{m/s^2}$, for which it has merged with the main branch. Forward and backward phase stepping results are depicted for both excitation levels. The test was initiated off resonance, near 10° and 170°, respectively. For the lower excitation level, only points on the main branch are obtained in this way. To obtain points on the isolated branch, the phase stepping was launched from the backbone (i. e., at phase resonance,

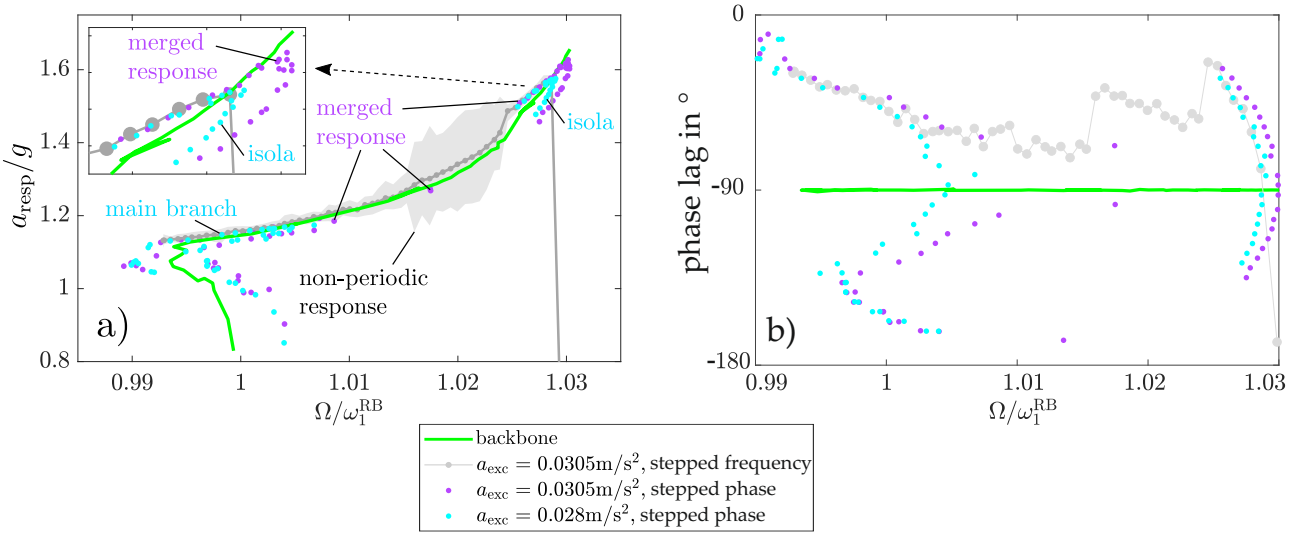

Fig. 11: Measured frequency response: (a) amplitude-frequency response; (b) phase-frequency response.

90°), from the upper point corresponding to $a_{\mathrm{exc}} = 0.028\ \mathrm{m/s^2}$. Again, forward and backward stepping was carried out. Near the expected turning points with respect to the phase lag, jumps occur to the main branch.
An advantage of the phase stepping is that points on the overhanging branch can also be obtained. A drawback is that jumps with respect to the frequency can appear. In contrast, a (more classical) frequency stepping has the advantage that such jumps do not appear, but the drawback that the overhanging branch cannot be reached In Fig. 11, frequency stepping results are shown only at $a_{\mathrm{exc}} = 0.0305\ \mathrm{m/s^2}$ for clarity. The results of the frequency stepping are largely consistent with those of the phase stepping, and complement the overall picture. A frequency window of non-periodic vibration response is encountered for $\Omega/\omega_1^{\mathrm{RB}} \in [1.015, 1.025]$. In Appendix B, additional results of the stepped sine tests are shown (for different excitation levels; highlighting the difference between forward and backward stepping). However, the picture is still incomplete, since parts of the isolated and the merged branch are missed. To obtain the remaining portions of the bifurcation diagram, some form of control-based continuation could be useful.
Using the method described in Section 2, frequency response branches according to Single-Nonlinear-Mode Theory were obtained. The results are illustrated in Fig. 12 (NM-ROM), and compared to the experimentally obtained frequency response data (reference), for the two different excitation levels. To obtain a better visualization of the NM-ROM results, the modal properties were interpolated with respect to the amplitude. Due to the discontinuities, typical of real measurements (contaminated with finite uncertainty), the interpolation causes some artificial loops/singularities. Otherwise, the results are in very good agreement. In particular, the qualitative outcome, isolated vs. merged branch, is in perfect alignment. This further supports the hypothesis that the experimentally observed isolated branches are in fact due to nonlinear damping and not due to resonant modal interaction.

6 Conclusions

Two important conclusions are drawn from the present work. First, tracking phase-resonant backbones, which has recently become very popular for the identification of amplitude-dependent modal properties, is also useful for the analysis of isolated frequency response branches. The ranges of the excitation level, which lead to the emergence / vanishing of isolated branches are directly obtained. The acquired vibration data can also be used to estimate the contributions of individual harmonics of different linear modes to the mechanical energy, which permits to detect and, if applicable, characterize resonant modal interactions. In the absence of strong modal interactions, a meaningful modal damping ratio can be obtained, which permits to analyze whether amplitude-dependent damping is responsible for the formation of the isolated branches. One should remark that the last two points, the harmonic and modal contributions to the mechanical energy, and the modal damping ratio, generally require that the vibration is measured with a sufficiently large number of properly placed sensors. The proposed method would not be conceivable without mature feedback-controllers for phase and amplitude.
The second conclusion refers to the observations made for the specific test rig. Strong evidence was established that the isolated branches are actually due to nonlinear damping, whereas resonant modal interactions were expected to

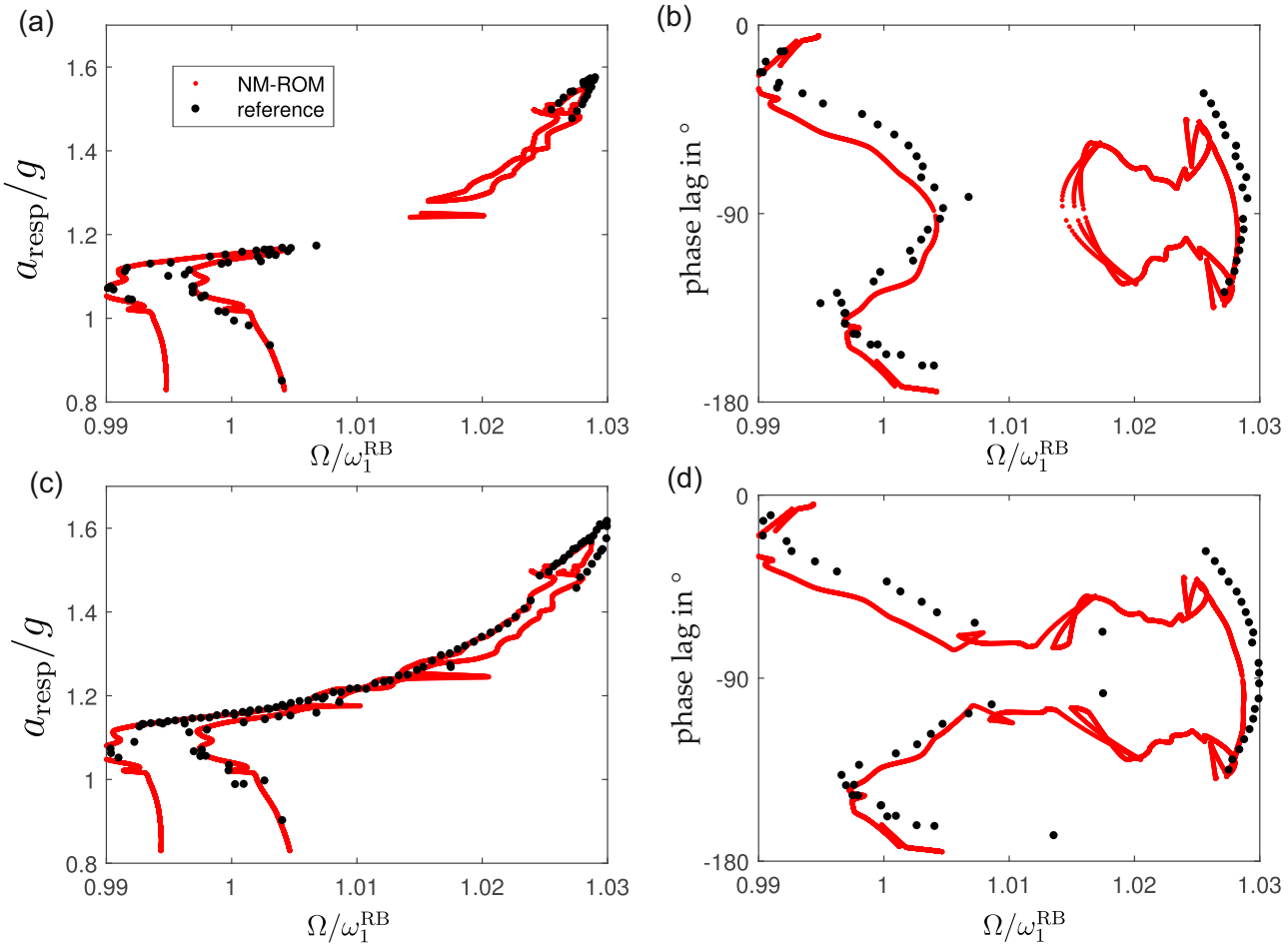

Fig. 12: Validation of Single-Nonlinear-Mode Theory: (a) amplitude- and (b) phase-frequency response for $a_{\mathrm{exc}} = 0.280\ \mathrm{m/s^2}$; (c) amplitude- and (b) phase-frequency response for $a_{\mathrm{exc}} = 0.305\ \mathrm{m/s^2}$. NM-ROM: synthesis obtained using identified nonlinear-mode model. Reference: directly measured frequency response data from Fig. 11. The legend in (a) applies to all sub-figures.

be responsible according to the model. This qualitative discrepancy is attributed to the invalidity of the linear modal damping assumption, if the real test rig features frictional connections. In addition, the increased damping in the nonlinear regime has the ability to suppress internal resonance phenomena. It should be stressed that the design intent was to minimize the nonlinear effects of these connections. Becoming able to predict this behavior is regarded as an ambitious and relevant objective of future research. With the presently available methods, it appears possible to *reproduce* complicated dynamics of assemblies comprising a single bolted joint only; an actual *prediction* of complicated dynamics does not seem possible today, especially not in the case of multiple joints or jointed structures undergoing recurrent impacts.

A potential limitation of the proposed procedure are test cases, where both nonlinear damping and internal resonance are responsible for the formation of isolated branches. Whether such a test case of engineering relevance exists, or these two mechanisms exclude each other in almost all cases, is an open question. Lastly, although the performance of the employed controllers was deemed acceptable for the given purpose, future research should be directed towards systematic control design, so that the tuning effort is reduced, excitation level control becomes feasible also in strongly modulated response regimes and higher excitation harmonics can be suppressed in more critical situations.

Authors' Contributions

Lukas Woiwode: research implementation; writing
Malte Krack: research concept; supervision; writing

Acknowledgements

The authors are grateful for the funding received by the Deutsche Forschungsgemeinschaft (DFG, German Research Foundation) [Projects 438529800, 495957501].

Supplementary Material

The measurement data is available in a repository via https://doi.org/10.18419/darus-4504. Besides measurement data, you also find CAD files and technical drawings, as well as a PDF indicating the measurement points there. The post-processing methods are provided via GitHub at https://github.com/maltekrack/NLtest. These load the data and generate plots similar to those in the article.

Appendix

A Dimensions of test rig

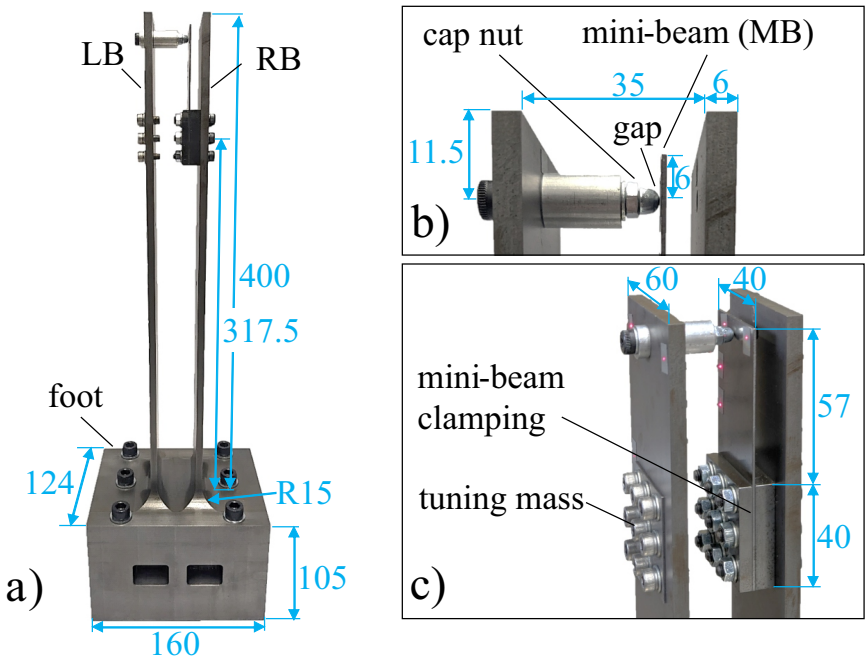

Fig. A.1: Variant of Fig. 8a-c with dimensions in mm.

B Additional results of the stepped sine tests

In Fig. B.1, additional results of the stepped sine tests are shown. Apparently, a window of non-periodic response appears also for $a_{\mathrm{exc}} = 0.02\ \mathrm{m/s^2}$ (Fig. B.1a). Also, the initial softening causes a difference between forward and backward stepping (Fig. B.1b).

References

[1] A. H. Nayfeh, D. T. Mook, Nonlinear Oscillations, Vol. 1979, John Wiley & Sons, New York.

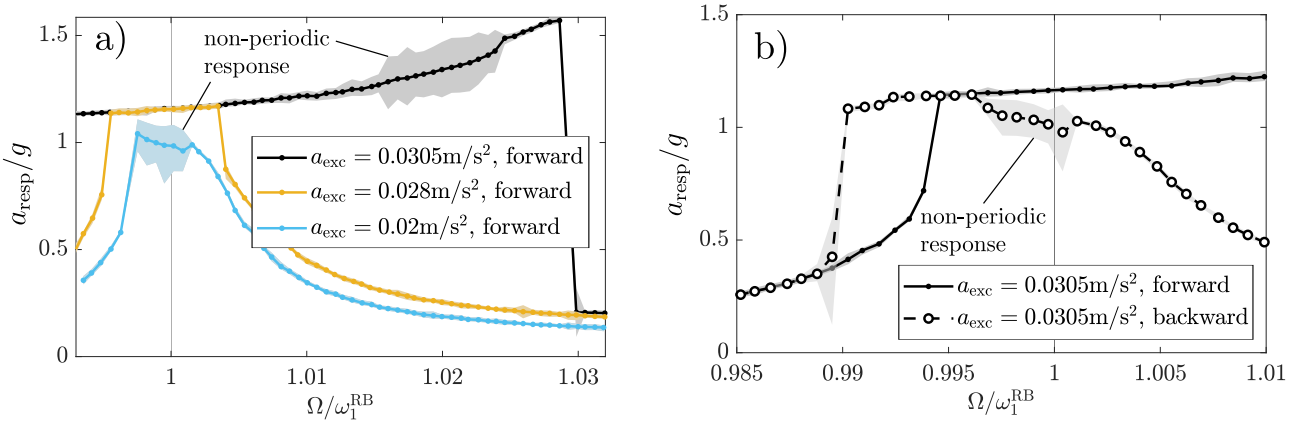

Fig. B.1: Additional results of the stepped sine tests: (a) forward stepping for different excitation levels; (b) forward vs. backward stepping at high excitation level.

[2] G. Habib, G. I. Cirillo, G. Kerschen, Isolated resonances and nonlinear damping, Nonlinear Dynamics 93 (3) (2018) 979–994. doi:10.1007/s11071-018-4240-z.
URL https://doi.org/10.1007/s11071-018-4240-z

[3] F. Mangussi, D. H. Zanette, Internal resonance in a vibrating beam: A zoo of nonlinear resonance peaks, PLOS ONE 11 (9) (2016) e0162365. doi:10.1371/journal.pone.0162365.
URL https://doi.org/10.1371/journal.pone.0162365

[4] L. Kloda, S. Lenci, J. Warminski, Z. Szmit, Flexural–flexural internal resonances 3:1 in initially straight, extensible timoshenko beams with an axial spring, Vibro-Impact Systems 527 (2022) 116809. doi:10.1016/j.jsv.2022.116809.
URL https://www.sciencedirect.com/science/article/pii/S0022460X22000608

[5] R. J. Kuether, L. Renson, T. Detroux, C. Grappasonni, G. Kerschen, M. S. Allen, Nonlinear normal modes, modal interactions and isolated resonance curves, Journal of Sound and Vibration 351 (2015) 299–310. doi:10.1016/j.jsv.2015.04.035.

[6] T. L. Hill, S. A. Neild, A. Cammarano, An analytical approach for detecting isolated periodic solution branches in weakly nonlinear structures, Journal of Sound and Vibration 379 (2016) 150–165. doi:10.1016/j.jsv.2016.05.030.
URL https://www.sciencedirect.com/science/article/pii/S0022460X16301663

[7] M. Cenedese, G. Haller, How do conservative backbone curves perturb into forced responses? a melnikov function analysis, Proceedings of the Royal Society A: Mathematical, Physical and Engineering Sciences 476 (2234) (2020) 20190494. doi:10.1098/rspa.2019.0494.

[8] L. Renson, T. L. Hill, D. A. Ehrhardt, D. A. W. Barton, S. A. Neild, Force appropriation of nonlinear structures, Proceedings of the Royal Society A: Mathematical, Physical and Engineering Sciences 474 (2214) (2018) 20170880. doi:10.1098/rspa.2017.0880.

[9] T. Heinze, L. Panning-von Scheidt, J. Wallaschek, Global detection of detached periodic solution branches of friction-damped mechanical systems, Nonlinear Dynamics 99 (2019) 1841–1870. doi:10.1007/s11071-019-05425-4.

[10] P. R. Sethna, A. K. Bajaj, Bifurcations in dynamical systems with internal resonance, Journal of Applied Mechanics 45 (4) (1978) 895–902. doi:10.1115/1.3424438.

[11] G. Mustafa, A. Ertas, Dynamics and bifurcations of a coupled column-pendulum oscillator, Vibro-Impact Systems 182 (3) (1995) 393–413. doi:10.1006/jsvi.1995.0207.
URL https://www.sciencedirect.com/science/article/pii/S0022460X85702076

[12] A. Y. T. Leung, T. C. Fung, Non-linear steady state vibration and dynamic snap through of shallow arch beams, Earthquake Engineering & Structural Dynamics 19 (3) (1990) 409–430. doi:10.1002/eqe.4290190309.

[13] D. A. Ehrhardt, T. L. Hill, S. A. Neild, Experimentally measuring an isolated branch of nonlinear normal modes, Vibro-Impact Systems 457 (2019) 213–226. doi:10.1016/j.jsv.2019.06.006.
URL https://www.sciencedirect.com/science/article/pii/S0022460X19303372

[14] A. D. Shaw, T. L. Hill, S. A. Neild, M. I. Friswell, Periodic responses of a structure with 3:1 internal resonance, Mechanical Systems and Signal Processing 81 (2016) 19–34. doi:10.1016/j.ymssp.2016.03.008.

[15] G. Gatti, M. J. Brennan, Inner detached frequency response curves: an experimental study, Journal of Sound and Vibration 396 (2017) 246–254. doi:10.1016/j.jsv.2017.02.008.

[16] T. Detroux, J.-P. Noël, L. N. Virgin, G. Kerschen, Experimental study of isolas in nonlinear systems featuring modal interactions, PLOS ONE 13 (3) (2018) e0194452. doi:10.1371/journal.pone.0194452.

[17] L. Renson, A. D. Shaw, D. Barton, S. A. Neild, Application of control-based continuation to a nonlinear structure with harmonically coupled modes, Mechanical Systems and Signal Processing 120 (2019) 449–464.

[18] E. Bureau, F. Schilder, M. Elmegård, I. F. Santos, J. J. Thomsen, J. Starke, Experimental bifurcation analysis of an impact oscillator—determining stability, Journal of Sound and Vibration 333 (21) (2014) 5464–5474. doi:10.1016/j.jsv.2014.05.032.

[19] D. A. W. Barton, B. P. Mann, S. G. Burrow, Control-based continuation for investigating nonlinear experiments, Journal of Vibration and Control 18 (4) (2011) 509–520. doi:10.1177/1077546310384004.

[20] S. Mojrzisch, J. Wallaschek, J. Bremer, An experimental method for the phase controlled frequency response measurement of nonlinear vibration systems, PAMM 12 (1) (2012) 253–254. doi:10.1002/pamm.201210117.

[21] S. Peter, R. I. Leine, Excitation power quantities in phase resonance testing of nonlinear systems with phase-locked-loop excitation, Mechanical Systems and Signal Processing 96 (Supplement C) (2017) 139–158. doi:10.1016/j.ymssp.2017.04.011.

[22] V. Denis, M. Jossic, C. Giraud-Audine, B. Chomette, A. Renault, O. Thomas, Identification of nonlinear modes using phase-locked-loop experimental continuation and normal form, Mechanical Systems and Signal Processing 106 (2018) 430–452. doi:10.1016/j.ymssp.2018.01.014.

[23] S. Peter, M. Scheel, M. Krack, R. I. Leine, Synthesis of nonlinear frequency responses with experimentally extracted nonlinear modes, Mechanical Systems and Signal Processing 101 (2018) 498–515. doi:10.1016/j.ymssp.2017.09.014.

[24] M. Scheel, S. Peter, R. I. Leine, M. Krack, A phase resonance approach for modal testing of structures with nonlinear dissipation, Journal of Sound and Vibration 435 (2018) 56–73. doi:10.1016/j.jsv.2018.07.010.

[25] S. Schwarz, L. Kohlmann, A. Hartung, J. Gross, M. Scheel, M. Krack, Validation of a turbine blade component test with frictional contacts by phase-locked-loop and force-controlled measurements, J. Eng. Gas Turbines Power (2019) 10ppdoi:10.1115/1.4044772.

[26] A. Givois, J.-J. Tan, C. Touzé, O. Thomas, Backbone curves of coupled cubic oscillators in one-to-one internal resonance: bifurcation scenario, measurements and parameter identification, Meccanica 55 (3) (2020) 481–503. doi:10.1007/s11012-020-01132-2.
URL https://doi.org/10.1007/s11012-020-01132-2

[27] G. Abeloos, L. Renson, C. Collette, G. Kerschen, Stepped and swept control-based continuation using adaptive filtering, Nonlinear Dynamics (2021). doi:10.1007/s11071-021-06506-z.
URL https://doi.org/10.1007/s11071-021-06506-z

[28] F. Müller, L. Woiwode, J. Gross, M. Scheel, M. Krack, Nonlinear damping quantification from phase-resonant tests under base excitation, Mechanical Systems and Signal Processing (2022). doi:10.1016/j.ymssp.2022.109170.
URL https://doi.org/10.1016/j.ymssp.2022.109170

[29] W. Szemplinska-Stupnicka, The modified single mode method in the investigations of the resonant vibrations of non-linear systems, Journal of Sound and Vibration 63 (4) (1979) 475–489. doi:10.1016/0022-460X(79)90823-X.
URL http://dx.doi.org/10.1016/0022-460X(79)90823-X

[30] M. Krack, J. Gross, Harmonic Balance for Nonlinear Vibration Problems, Springer, 2019. doi:10.1007/978-3-030-14023-6.

[31] C. Monjaraz-Tec, L. Kohlmann, S. Schwarz, A. Hartung, J. Gross, M. Krack, Prediction and validation of the strongly modulated forced response of two beams undergoing frictional impacts, Mechanical Systems and Signal Processing 180 (2022) 109410. doi:10.1016/j.ymssp.2022.109410.
URL https://www.sciencedirect.com/science/article/pii/S0888327022005362

[32] M. R. Brake (Ed.), The Mechanics of Jointed Structures: Recent Research and Open Challenges for Developing Predictive Models for Structural Dynamics, Springer International Publishing, Cham, 2018.

[33] J. M. Londoño, S. A. Neild, J. E. Cooper, Identification of backbone curves of nonlinear systems from resonance decay responses, Journal of Sound and Vibration 348 (2015) 224–238. doi:10.1016/j.jsv.2015.03.015.